Measurement of time-dependent *CP* asymmetries in $B^0 \to K_S^0 \eta \gamma$ decays

H. Nakano,[83] A. Ishikawa,[83] K. Sumisawa,[18,14] H. Yamamoto,[83] I. Adachi,[18,14] H. Aihara,[85] S. Al Said,[78,37] D. M. Asner,[3] V. Aulchenko,[4,66] T. Aushev,[55] R. Ayad,[78] V. Babu,[79] I. Badrees,[78,36] V. Bansal,[68] P. Behera,[24] C. Beleño,[13] B. Bhuyan,[22] T. Bilka,[5] J. Biswal,[32] A. Bozek,[62] M. Bračko,[49,32] D. Červenkov,[5] V. Chekelian,[50] B. G. Cheon,[16] K. Chilikin,[44] K. Cho,[38] S.-K. Choi,[15] Y. Choi,[77] S. Choudhury,[23] D. Cinabro,[89] S. Cunliffe,[7] N. Dash,[21] S. Di Carlo,[42] Z. Doležal,[5] S. Eidelman,[4,66] J. E. Fast,[68] T. Ferber,[7] B. G. Fulsom,[68] R. Garg,[69] V. Gaur,[88] N. Gabyshev,[4,66] A. Garmash,[4,66] M. Gelb,[34] A. Giri,[23] P. Goldenzweig,[34] Y. Guan,[25,18] E. Guido,[30] J. Haba,[18,14] T. Hara,[18,14] K. Hayasaka,[64] H. Hayashii,[59] M. T. Hedges,[17] S. Hirose,[56] W.-S. Hou,[61] T. Iijima,[57,56] K. Inami,[56] G. Inguglia,[7] R. Itoh,[18,14] M. Iwasaki,[67] Y. Iwasaki,[18] W. W. Jacobs,[25] I. Jaegle,[9] H. B. Jeon,[41] S. Jia,[2] Y. Jin,[85] T. Julius,[51] A. B. Kaliyar,[24] G. Karyan,[7] T. Kawasaki,[64] C. Kiesling,[50] D. Y. Kim,[75] H. J. Kim,[41] J. B. Kim,[39] K. T. Kim,[39] S. H. Kim,[16] K. Kinoshita,[6] P. Kodyš,[5] S. Korpar,[49,32] D. Kotchetkov,[17] P. Križan,[45,32] R. Kroeger,[52] P. Krokovny,[4,66] T. Kuhr,[46] R. Kulasiri,[35] T. Kumita,[87] Y.-J. Kwon,[91] J. S. Lange,[11] I. S. Lee,[16] S. C. Lee,[41] L. K. Li,[26] Y. Li,[88] Y. B. Li,[70] L. Li Gioi,[50] J. Libby,[24] D. Liventsev,[88,18] M. Lubej,[32] T. Luo,[10] J. MacNaughton,[18] M. Masuda,[84] T. Matsuda,[53] M. Merola,[29,58] K. Miyabayashi,[59] H. Miyata,[64] R. Mizuk,[44,54,55] G. B. Mohanty,[79] H. K. Moon,[39] R. Mussa,[30] E. Nakano,[67] M. Nakao,[18,14] T. Nanut,[32] K. J. Nath,[22] Z. Natkaniec,[62] M. Nayak,[89,18] M. Niiyama,[40] S. Nishida,[18,14] S. Ogawa,[82] S. Okuno,[33] H. Ono,[63,64] P. Pakhlov,[44,54] G. Pakhlova,[44,55] B. Pal,[6] S. Pardi,[29] H. Park,[41] S. Paul,[81] T. K. Pedlar,[47] R. Pestotnik,[32] L. E. Piilonen,[88] V. Popov,[44,55] M. Ritter,[46] A. Rostomyan,[7] G. Russo,[29] D. Sahoo,[79] Y. Sakai,[18,14] M. Salehi,[48,46] S. Sandilya,[6] L. Santelj,[18] T. Sanuki,[83] V. Savinov,[71] O. Schneider,[43] G. Schnell,[1,20] C. Schwanda,[27] A. J. Schwartz,[6] Y. Seino,[64] K. Senyo,[90] M. E. Sevior,[51] V. Shebalin,[4,66] C. P. Shen,[2] T.-A. Shibata,[86] N. Shimizu,[85] J.-G. Shiu,[61] B. Shwartz,[4,66] F. Simon,[50,80] A. Sokolov,[28] E. Solovieva,[44,55] S. Stanič,[65] M. Starič,[32] J. F. Strube,[68] M. Sumihama,[12] T. Sumiyoshi,[87] M. Takizawa,[74,19,72] U. Tamponi,[30] K. Tanida,[31] F. Tenchini,[51] K. Trabelsi,[18,14] M. Uchida,[86] T. Uglov,[44,55] S. Uno,[18,14] P. Urquijo,[51] Y. Usov,[4,66] C. Van Hulse,[1] G. Varner,[17] V. Vorobyev,[4,66] A. Vossen,[8] B. Wang,[6] C. H. Wang,[60] M.-Z. Wang,[61] P. Wang,[26] X. L. Wang,[10] M. Watanabe,[64] E. Widmann,[76] E. Won,[39] H. Ye,[7] C. Z. Yuan,[26] Y. Yusa,[64] S. Zakharov,[44,55] Z. P. Zhang,[73] V. Zhilich,[4,66] V. Zhukova,[44,54] V. Zhulanov,[4,66] and A. Zupanc[45,32]

(Belle Collaboration)

[1]*University of the Basque Country UPV/EHU, 48080 Bilbao*
[2]*Beihang University, Beijing 100191*
[3]*Brookhaven National Laboratory, Upton, New York 11973*
[4]*Budker Institute of Nuclear Physics SB RAS, Novosibirsk 630090*
[5]*Faculty of Mathematics and Physics, Charles University, 121 16 Prague*
[6]*University of Cincinnati, Cincinnati, Ohio 45221*
[7]*Deutsches Elektronen–Synchrotron, 22607 Hamburg*
[8]*Duke University, Durham, North Carolina 27708*
[9]*University of Florida, Gainesville, Florida 32611*
[10]*Key Laboratory of Nuclear Physics and Ion-beam Application (MOE) and Institute of Modern Physics,*
Fudan University, Shanghai 200443
[11]*Justus-Liebig-Universität Gießen, 35392 Gießen*
[12]*Gifu University, Gifu 501-1193*
[13]*II. Physikalisches Institut, Georg-August-Universität Göttingen, 37073 Göttingen*
[14]*SOKENDAI (The Graduate University for Advanced Studies), Hayama 240-0193*
[15]*Gyeongsang National University, Chinju 660-701*
[16]*Hanyang University, Seoul 133-791*
[17]*University of Hawaii, Honolulu, Hawaii 96822*
[18]*High Energy Accelerator Research Organization (KEK), Tsukuba 305-0801*
[19]*J-PARC Branch, KEK Theory Center, High Energy Accelerator Research Organization (KEK),*
Tsukuba 305-0801
[20]*IKERBASQUE, Basque Foundation for Science, 48013 Bilbao*
[21]*Indian Institute of Technology Bhubaneswar, Satya Nagar 751007*
[22]*Indian Institute of Technology Guwahati, Assam 781039*
[23]*Indian Institute of Technology Hyderabad, Telangana 502285*
[24]*Indian Institute of Technology Madras, Chennai 600036*
[25]*Indiana University, Bloomington, Indiana 47408*

092003-1

[26]Institute of High Energy Physics, Chinese Academy of Sciences, Beijing 100049

[27]Institute of High Energy Physics, Vienna 1050

[28]Institute for High Energy Physics, Protvino 142281

[29]INFN–Sezione di Napoli, 80126 Napoli

[30]INFN–Sezione di Torino, 10125 Torino

[31]Advanced Science Research Center, Japan Atomic Energy Agency, Naka 319-1195

[32]J. Stefan Institute, 1000 Ljubljana

[33]Kanagawa University, Yokohama 221-8686

[34]Institut für Experimentelle Teilchenphysik, Karlsruher Institut für Technologie, 76131 Karlsruhe

[35]Kennesaw State University, Kennesaw, Georgia 30144

[36]King Abdulaziz City for Science and Technology, Riyadh 11442

[37]Department of Physics, Faculty of Science, King Abdulaziz University, Jeddah 21589

[38]Korea Institute of Science and Technology Information, Daejeon 305-806

[39]Korea University, Seoul 136-713

[40]Kyoto University, Kyoto 606-8502

[41]Kyungpook National University, Daegu 702-701

[42]LAL, Univ. Paris-Sud, CNRS/IN2P3, Université Paris-Saclay, Orsay

[43]École Polytechnique Fédérale de Lausanne (EPFL), Lausanne 1015

[44]P.N. Lebedev Physical Institute of the Russian Academy of Sciences, Moscow 119991

[45]Faculty of Mathematics and Physics, University of Ljubljana, 1000 Ljubljana

[46]Ludwig Maximilians University, 80539 Munich

[47]Luther College, Decorah, Iowa 52101

[48]University of Malaya, 50603 Kuala Lumpur

[49]University of Maribor, 2000 Maribor

[50]Max-Planck-Institut für Physik, 80805 München

[51]School of Physics, University of Melbourne, Victoria 3010

[52]University of Mississippi, University, Mississippi 38677

[53]University of Miyazaki, Miyazaki 889-2192

[54]Moscow Physical Engineering Institute, Moscow 115409

[55]Moscow Institute of Physics and Technology, Moscow Region 141700

[56]Graduate School of Science, Nagoya University, Nagoya 464-8602

[57]Kobayashi-Maskawa Institute, Nagoya University, Nagoya 464-8602

[58]Università di Napoli Federico II, 80055 Napoli

[59]Nara Women's University, Nara 630-8506

[60]National United University, Miao Li 36003

[61]Department of Physics, National Taiwan University, Taipei 10617

[62]H. Niewodniczanski Institute of Nuclear Physics, Krakow 31-342

[63]Nippon Dental University, Niigata 951-8580

[64]Niigata University, Niigata 950-2181

[65]University of Nova Gorica, 5000 Nova Gorica

[66]Novosibirsk State University, Novosibirsk 630090

[67]Osaka City University, Osaka 558-8585

[68]Pacific Northwest National Laboratory, Richland, Washington 99352

[69]Panjab University, Chandigarh 160014

[70]Peking University, Beijing 100871

[71]University of Pittsburgh, Pittsburgh, Pennsylvania 15260

[72]Theoretical Research Division, Nishina Center, RIKEN, Saitama 351-0198

[73]University of Science and Technology of China, Hefei 230026

[74]Showa Pharmaceutical University, Tokyo 194-8543

[75]Soongsil University, Seoul 156-743

[76]Stefan Meyer Institute for Subatomic Physics, Vienna 1090

[77]Sungkyunkwan University, Suwon 440-746

[78]Department of Physics, Faculty of Science, University of Tabuk, Tabuk 71451

[79]Tata Institute of Fundamental Research, Mumbai 400005

[80]Excellence Cluster Universe, Technische Universität München, 85748 Garching

[81]Department of Physics, Technische Universität München, 85748 Garching

[82]Toho University, Funabashi 274-8510

[83]Department of Physics, Tohoku University, Sendai 980-8578

[84]Earthquake Research Institute, University of Tokyo, Tokyo 113-0032

[85]Department of Physics, University of Tokyo, Tokyo 113-0033

^{86}Tokyo Institute of Technology, Tokyo 152-8550
^{87}Tokyo Metropolitan University, Tokyo 192-0397
^{88}Virginia Polytechnic Institute and State University, Blacksburg, Virginia 24061
^{89}Wayne State University, Detroit, Michigan 48202
^{90}Yamagata University, Yamagata 990-8560
^{91}Yonsei University, Seoul 120-749

We report a measurement of time-dependent CP violation parameters in $B^0 \to K_S^0 \eta \gamma$ decays. The study is based on a data sample, containing $772 \times 10^6 B\bar{B}$ pairs, that was collected at the $\Upsilon(4S)$ resonance with the Belle detector at the KEKB asymmetric-energy $e^+ e^-$ collider. We obtain the CP violation parameters of $\mathcal{S} = -1.32 \pm 0.77(\text{stat}) \pm 0.36(\text{syst})$ and $\mathcal{A} = -0.48 \pm 0.41(\text{stat}) \pm 0.07(\text{syst})$ for the invariant mass of the $K_S^0 \eta$ system up to 2.1 GeV/c^2.

I. INTRODUCTION

The radiative $b \to s\gamma$ decay proceeds dominantly via one-loop electromagnetic penguin diagrams at lowest order in the standard model (SM). Since heavy unobserved particles might enter in the loop, such decays are sensitive to new physics (NP). Precision measurements of the branching fraction for $B \to X_s\gamma$ by CLEO [1], *BABAR* [2–4] and Belle [5,6] are consistent with SM predictions [7,8] and give a strong constraint to NP models [9]. Another important observable that is sensitive to NP signatures in the $b \to s\gamma$ process is the photon polarization. Within the SM, the photon is mostly produced with left-handed polarization; the right-handed contribution is suppressed by m_s/m_b at leading order, where m_s (m_b) is the strange (bottom) quark mass. Various NP models, such as supersymmetry [10–15], left-right symmetric models [16] and extra dimensions [17–22], allow right-handed currents in the loops and hence can enhance the right-handed photon contribution [23–27]. Thus, a measurement of the photon polarization in the $b \to s\gamma$ process is an important tool to search for NP.

Several methods have been proposed to measure the photon polarization in the $b \to s\gamma$ process. A measurement of time-dependent CP violation in $B^0 \to P_1^0 P_2^0 \gamma$ is the most promising one, where P_1^0 and P_2^0 are scalar or pseudoscalar mesons and the $P_1^0 P_2^0$ system is a CP eigenstate [28,29]. As the left- (right-)handed photon contributions are suppressed in B^0 ($\bar{B}^0$) decays in the SM, an interference between $\bar{B}^0 \to P_1^0 P_2^0 \gamma_{L(R)}$ and $B^0 \to P_1^0 P_2^0 \gamma_{L(R)}$ can generate a small mixing-induced CP violation parameterized by $\mathcal{S} \sim -2\xi_{CP}(m_s/m_b)\sin 2\phi_1 \sim -0.02\xi_{CP}$. Here, ξ_{CP} is the

CP eigenvalue of the $P_1^0 P_2^0$ system, and ϕ_1 is an interior angle of the Cabibbo-Kobayashi-Maskawa unitarity triangle [30,31], defined as $\phi_1 \equiv \arg[-V_{cd}V_{cb}^*/V_{td}V_{tb}^*]$. Potential contributions from NP-associated right-handed currents could enhance the value of S in the $B^0 \to P_1^0 P_2^0 \gamma$ process [28,32–41].

At Belle and *BABAR*, the CP violation parameters for the $b \to s\gamma$ transition were measured in the decays of $B^0 \to K_S^0 \pi^0 \gamma$ including $K^{*0} \to K_S^0 \pi^0$ [42,43], $B^0 \to K_S^0 \eta \gamma$ [44], $B^0 \to K_S^0 \rho^0 \gamma$ [45,46], and $B^0 \to K_S^0 \phi \gamma$ [47]. All results are consistent with the SM prediction within the uncertainties [48–53]. In this paper, we report the first measurement of time-dependent CP violation in $B^0 \to K_S^0 \eta \gamma$ at Belle. The study is based on the full data sample of 711 fb^{-1} containing $772 \times 10^6 B\bar{B}$ pairs recorded at the $\Upsilon(4S)$ resonance with the Belle detector [54] at the KEKB $e^+ e^-$ collider [55].

II. TIME-DEPENDENT CP VIOLATION

At the KEKB asymmetric-energy collider (3.5 GeV e^+ on 8.0 GeV e^-), the $\Upsilon(4S)$ is produced with a Lorentz boost of $\beta\gamma = 0.425$ nearly along the z axis, which is antiparallel to the e^+ beam direction. In the decay chain $\Upsilon(4S) \to B^0\bar{B}^0 \to f_{\text{rec}}f_{\text{tag}}$, one of the B mesons decays at proper time t_{rec} to a final state f_{rec} (our signal mode), and the other (B_{tag}) decays at proper time t_{tag} to a final state f_{tag} that is used to determine the flavor of the signal B meson. The distribution of the proper time difference $\Delta t = t_{\text{rec}} - t_{\text{tag}}$ is given by

$$\mathcal{P}(\Delta t) = \frac{e^{-|\Delta t|/\tau_{B^0}}}{4\tau_{B^0}}\{1 + q[\mathcal{S}\sin(\Delta m_d \Delta t) \tag{1}$$

$$+ \mathcal{A}\cos(\Delta m_d \Delta t)]\}, \tag{2}$$

where $\mathcal{S}$ ($\mathcal{A}$) is the mixing-induced (direct) CP violation parameter, τ_{B^0} is the B^0 lifetime, Δm_d is the mass difference

between the two B^0 mass eigenstates, and $q = +1$ (-1) is the b-flavor charge when the tagging B meson is a B^0 ($\bar{B}^0$). Since the B^0 and $\bar{B}^0$ mesons are approximately at rest in the $\Upsilon(4S)$ center-of-mass (CM) frame, Δt can be determined from the displacement in z in the laboratory frame between the f_{rec} and f_{tag} decay vertices: $\Delta t \simeq (z_{\text{rec}} - z_{\text{tag}})/\beta\gamma c \equiv \Delta z/\beta\gamma c$, where z_{rec} and z_{tag} are the decay positions along the z axis of the signal and tag-side B mesons.

III. BELLE DETECTOR

The Belle detector [54] is a large-solid-angle magnetic spectrometer that consists of a silicon vertex detector (SVD), a 50-layer central drift chamber (CDC), an array of aerogel threshold Cherenkov counters (ACC), a barrel-like arrangement of time-of-flight scintillation counters (TOF), and an electromagnetic caloriemeter (ECL) comprised of CsI(Tl) crystals. All these detector components are located inside a superconducting solenoid coil that provides a 1.5 T magnetic field. An iron flux-return located outside of the coil is instrumented with resistive plate chambers to detect K_L^0 mesons and muons. Two inner detector configurations were used: A 2.0 cm radius beampipe and a 3-layer SVD was used for the first sample of $152 \times 10^6 B\bar{B}$ pairs (SVD1), while a 1.5 cm radius beampipe, a 4-layer SVD and a small-inner-cell CDC were used to record the remaining $620 \times 10^6 B\bar{B}$ pairs (SVD2) [56].

IV. EVENT SELECTION

The most energetic isolated cluster in the ECL in the CM frame of an event that is not associated with any charged tracks reconstructed in the SVD and CDC is selected as the prompt photon. Its energy must lie between 1.8 and 3.4 GeV. We require that its shower shape be consistent with an electromagnetic shower by imposing the criterion $E_9/E_{25} > 0.95$ for the ratio of energy deposits in a 3×3 array of CsI(Tl) crystals to that in a 5×5 array, both centered on the crystal with the largest energy deposit. To reduce contamination from the decays $\pi^0 \to \gamma\gamma$ or $\eta \to \gamma\gamma$, the prompt photon candidate is paired with all other photons in the event with energy exceeding 40 MeV in the laboratory frame. We reject the event if the pair is consistent with the above decays, based on a likelihood constructed from the invariant mass, the energy and polar angle of the second photon in the laboratory frame [57].

Neutral pion candidates are reconstructed from two photons whose energies exceed 50 MeV in the laboratory frame. We require the invariant mass of the photon pairs to lie between 114 and 147 MeV/c^2, which corresponds approximately to a $\pm3\sigma$ window in resolution about the nominal π^0 mass [58]. To reduce the combinatorial background, we retain candidates with a momentum greater than 100 MeV/c in the CM frame.

Charged particles, except for pions from K_S^0 decays, are required to have a distance of closest approach to the interaction point (IP) within 5.0 cm along the z axis and 0.5 cm in the transverse plane. Charged kaons and pions are identified with a likelihood ratio constructed from specific ionization measurements in the CDC, time-of-flight information from the TOF, and the number of photoelectrons in the ACC.

Neutral kaon (K_S^0) candidates are reconstructed from pairs of oppositely charged tracks, treated as pions, and identified by a multivariate analysis [59] based on two sets of input variables [60]. The first set that separates K_S^0 candidates from the combinatorial background are: (1) the K_S^0 momentum in the laboratory frame, (2) the distance along the z axis between the two track helices at their closest approach, (3) the flight length in the $x - y$ plane, (4) the angle between the K_S^0 momentum and the vector joining its decay vertex to the nominal IP, (5) the angle between the π momentum and the laboratory-frame direction of the K_S^0 in its rest frame, (6) the distances of closest approach in the $x - y$ plane between the IP and the pion helices, (7) the numbers of hits for axial and stereo wires in the CDC for each pion, and (8) the presence or absence of associated hits in the SVD for each pion. The second set of variables, which identifies $\Lambda \to p\pi^-$ background that has a similar long-lived topology, are: (1) particle identification information, momentum, and polar angles of the two daughter tracks in the laboratory frame, and (2) the invariant mass calculated with the proton- and pion-mass hypotheses for the two tracks. In total, the first and second sets comprise 13 and 7 input variables, respectively. The selected K_S^0 candidates are required to have an invariant mass within ±10 MeV/c^2 of the nominal value, corresponding to a $\pm3\sigma$ interval in mass resolution.

We reconstruct η candidates from the $\gamma\gamma$ and $\pi^+\pi^-\pi^0$ final states, denoted as $\eta_{2\gamma}$ and $\eta_{3\pi}$, respectively. For the $\eta_{2\gamma}$ mode, we require that the photon energy in the CM system be greater than 150 MeV. The candidates satisfying the di-photon invariant mass requirement of 510 MeV/$c^2 < M_{\gamma\gamma} < 575$ MeV/c^2 are retained. For the $\eta_{3\pi}$ mode, the invariant mass of the three-pion system is required to be in the range 537 MeV/$c^2 < M_{\pi\pi\pi} < 556$ MeV/c^2. These requirements correspond to about $\pm2\sigma$ windows in mass resolution.

We reconstruct B candidates by combining a K_S^0 with an η and a γ candidate. We form two kinematic variables to select B mesons: the energy difference $\Delta E \equiv E_B^{\text{CM}} - E_{\text{beam}}^{\text{CM}}$ and the beam-energy constrained mass $M_{\text{bc}} \equiv \sqrt{(E_{\text{beam}}^{\text{CM}}/c^2)^2 - (p_B^{\text{CM}}/c)^2}$, where $E_{\text{beam}}^{\text{CM}}$ is the beam energy, and E_B^{CM} and p_B^{CM} are the energy and momentum, respectively, of the B candidate in the CM system. We define the signal region in ΔE and M_{bc} for the measurement of CP violation as -0.15 GeV $< \Delta E < 0.08$ GeV and

$5.27 \text{ GeV}/c^2 < M_{\text{bc}} < 5.29 \text{ GeV}/c^2$. To determine the signal fraction, a larger fitting region, $|\Delta E| < 0.5$ GeV and $5.20 \text{ GeV}/c^2 < M_{\text{bc}} < 5.29 \text{ GeV}/c^2$, is employed. The average number of *B* candidates in an event with at least one candidate is 1.47; this is primarily due to multiple η candidates. If there is more than one *B* candidate in the fitting region, the candidate whose η daughter's mass is closest to the nominal value is selected. If still necessary, the *B* candidate with the K_S^0 daughter's mass closest to the nominal value is retained.

V. BACKGROUND SUPPRESSION

To suppress the dominant $e^+e^- \to q\bar{q}$ ($q \in \{u, d, s, c\}$) continuum background, we use a neural network based on four input variables calculated in the CM frame: (1) the cosine of the angle between the *B* momentum and the *z* axis, (2) the likelihood ratio of modified Fox-Wolfram moments [61,62] that gives the strongest separation power, (3) the cosine of the angle between the third sphericity axes [63] calculated from the *B* candidate and all other particles in the rest of the event (ROE), and (4) the cosine of the angle between the first sphericity axis in the ROE and the *z* axis. The network is trained with a GEANT3-based Monte Carlo (MC) simulation [64]. The output variable, $\mathcal{O}_{\text{NB}}$, in the range $[-1, 1]$, is used as one of the variables to determine the signal fraction. To enable a simple analytical modeling, $\mathcal{O}_{\text{NB}}$ is transformed into

$$\mathcal{O}'_{\text{NB}} = \ln \frac{\mathcal{O}_{\text{NB}} - \mathcal{O}_{\text{NB}}^{\text{min}}}{\mathcal{O}_{\text{NB}}^{\text{max}} - \mathcal{O}_{\text{NB}}}, \qquad (3)$$

where $\mathcal{O}_{\text{NB}}^{\text{min}}$ and $\mathcal{O}_{\text{NB}}^{\text{max}}$ are chosen to be -0.7 and 0.935 (0.915), respectively, for the $\eta_{2\gamma}$ $(\eta_{3\pi})$ mode. The events with $\mathcal{O}_{\text{NB}} < \mathcal{O}_{\text{NB}}^{\text{min}}$ are discarded; this selection keeps 80% (73%) of the signal while removing 92% (95%) $q\bar{q}$ background for the $\eta_{2\gamma}$ $(\eta_{3\pi})$ mode.

The decay modes of the following *CP* eigenstates constitute peaking backgrounds: $B^0 \to J/\psi(\eta\gamma)K_S^0$, $B^0 \to a_X(\eta\pi^0)K_S^0$, $B^0 \to \bar{D}^0(K_S^0\eta)\pi^0$, $B^0 \to \bar{D}^0(K_S^0\eta)\eta$, $B^0 \to \bar{D}^0(K_S^0\pi^0)\eta$, and $B^0 \to \eta K_X(K_S^0\pi^0)$, where a_X and K_X represent a light unflavored resonance and a kaonic resonance, respectively. To suppress these backgrounds, we require $2.0 \text{ GeV}/c^2 < M_{\gamma\eta} < 2.9 \text{ GeV}/c^2$ or $M_{\gamma\eta} > 3.2 \text{ GeV}/c^2$ to eliminate $J/\psi \to \eta\gamma$ and $a_X \to \eta\pi^0$, $M_{K\eta} < 1.82 \text{ GeV}/c^2$ or $M_{K\eta} > 1.90 \text{ GeV}/c^2$ to remove $\bar{D}^0 \to K_S^0\eta$, and $M_{\gamma K} > 2.0 \text{ GeV}/c^2$ to suppress $K_X \to K_S^0\pi^0$ and $\bar{D}^0 \to K_S^0\pi^0$, where a soft photon from the π^0 decay is undetected.

One of the decays arising from the $b \to s\gamma$ transition, $B^0 \to K_S^0\pi^0\gamma$, is a major peaking background. This decay is exclusively reconstructed and rejected if the candidate is found to satisfy the following requirements:

$0.12 \text{ GeV}/c^2 < M_{\gamma\gamma} < 0.15 \text{ GeV}/c^2$, $1.6 \text{ GeV} < E_\gamma^{\text{CM}} < 3.4 \text{ GeV}$, $-0.20 \text{ GeV} < \Delta E < 0.10 \text{ GeV}$, and $M_{\text{bc}} > 5.27 \text{ GeV}/c^2$.

VI. HELICITY ANGLE AND MASS DISTRIBUTIONS

As the spin and invariant mass of the $K\eta$ system are not well known, we study $B^+ \to K^+\eta\gamma$ [65] assuming the isospin symmetry breaking to be small between $B^0 \to K^0\eta\gamma$ and $B^+ \to K^+\eta\gamma$ [66]. The selections on $B^+ \to K^+\eta\gamma$ are the same as those on $B^0 \to K_S^0\eta\gamma$ except for kaon selections. We define the helicity angle (θ_{hel}) as the angle between the *K* momentum and the opposite of the *B*-meson momentum in the $K\eta$ rest frame. The signal yields are extracted by fitting to ΔE and M_{bc} in bins of $\cos\theta_{\text{hel}}$ and the $K^+\eta$ invariant mass; later, the efficiency-corrected yield is obtained. We fit to the $\cos\theta_{\text{hel}}$ distribution with spin-1 and spin-2 hypotheses, as a spin-3 resonance in *B* decays is only found in a B_s^0 decay and is highly suppressed compared to the spin-1 states [68]. Figures 1 and 2 show the background-subtracted and efficiency-corrected θ_{hel} and invariant-mass distributions for $B^+ \to K^+\eta\gamma$. We find that the signal is concentrated in the region $M_{K\eta} < 2.1 \text{ GeV}/c^2$ and has the signature of a spin-1 system. From these studies, we apply two selection criteria,
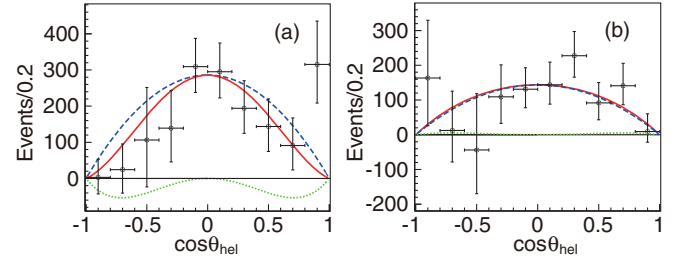

FIG. 1. Background-subtracted and efficiency-corrected helicity angle distributions of $B^+ \to K^+\eta\gamma$ for (a) $\eta_{2\gamma}$ and (b) $\eta_{3\pi}$ modes. The solid red curve shows the fit result, the dashed blue curve is the spin-1 component, and the dotted green line is the spin-2 component.
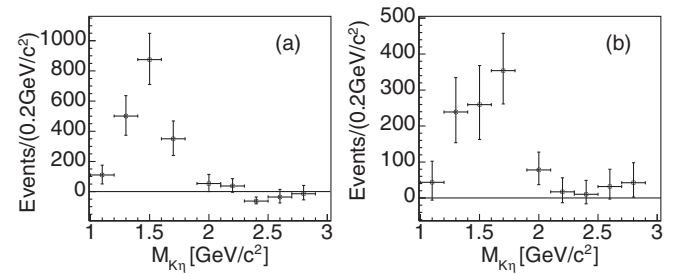

FIG. 2. Background-subtracted and efficiency-corrected invariant mass distributions of the $K^+\eta$ system for the (a) $\eta_{2\gamma}$ and (b) $\eta_{3\pi}$ modes.

$-0.7 < \cos\theta_{\text{hel}} < 0.9$ and $M_{K\eta} < 2.1$ GeV/c^2, to $B^0 \to K_S^0 \eta\gamma$ candidates to maximize the signal sensitivity.

VII. SIGNAL EXTRACTION

We extract the signal yield with a three-dimensional extended unbinned maximum-likelihood fit to ΔE, M_{bc}, and $\mathcal{O}'_{\text{NB}}$. For the signal ΔE–M_{bc} distribution, a two-dimensional histogram is used as the two variables have 40% correlation due to the imperfect energy measurement for the prompt photon. The $\mathcal{O}'_{\text{NB}}$ distribution is modeled with the sum of two bifurcated Gaussian functions sharing a common peak position and right-side width. For the $q\bar{q}$ background, the ΔE and M_{bc} distributions are parameterized by a second-order Chebyshev polynomial and an ARGUS function [69], respectively. The sum of a bifurcated Gaussian and a Gaussian function reproduces its $\mathcal{O}'_{\text{NB}}$ distribution. For background from B meson decays, the ΔE distribution is described by an exponential function; $\mathcal{O}'_{\text{NB}}$ is modeled with a bifurcated Gaussian function; the M_{bc} distribution is described by the sum of an ARGUS function and a Gaussian function. The fit results projected onto ΔE, M_{bc} and $\mathcal{O}'_{\text{NB}}$ are shown in Fig. 3. We obtain $69.5^{+13.4}_{-12.4}$ and $22.4^{+7.3}_{-6.4}$ signal events for the $\eta_{2\gamma}$ and $\eta_{3\pi}$ decay modes, respectively, with purities in the signal region of 28.4% and 22.5%.
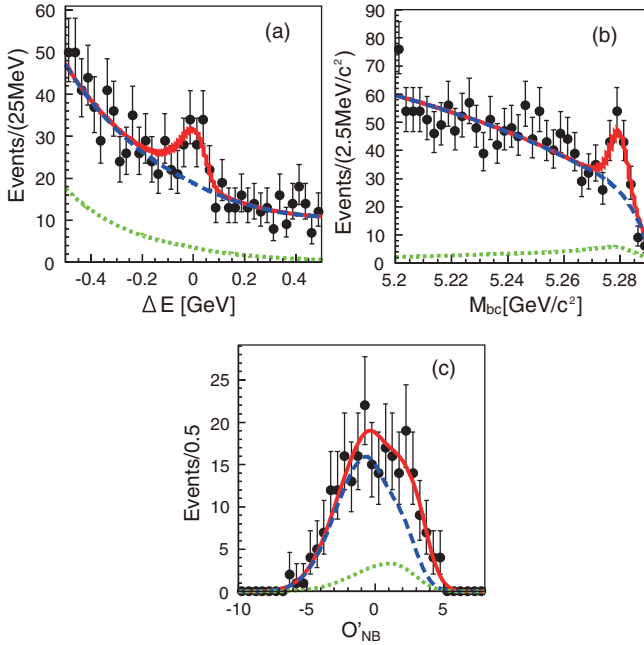

FIG. 3.   Projections of the three-dimensional fit onto: (a) ΔE in the M_{bc} signal region, (b) M_{bc} in the ΔE signal region and (c) $\mathcal{O}'_{\text{NB}}$ in the ΔE and M_{bc} signal regions. The solid red curves show the fit results, the dotted green curves represent $B\bar{B}$ background, and the dashed blue curves describe the total background.

VIII. FLAVOR TAGGING

The flavor of the B_{tag} meson is determined from inclusive properties of particles in the ROE based on a multi-dimensional likelihood method. The algorithm for flavor tagging is described in detail elsewhere [70]. Two parameters, q defined in Eq. (2) and r, are used to represent the tagging information. The parameter r is an event-by-event MC-determined flavor tagging quality factor that ranges from 0 for no flavor information to 1 for unambiguously determined flavor. The data are sorted into seven intervals of r in which the fractions of wrongly tagged B flavor (w_l, $l = 1, \ldots, 7$) as well as the differences between B^0 and $\bar{B}^0$ (Δw_l) are determined from self-tagged semi-leptonic and hadronic $b \to c$ decays. The total effective tagging efficiency, $\Sigma[f_l \times (1 - 2w_l)^2]$, where f_l is the fraction of events in category l, is determined to be $(29.8 \pm 0.4)\%$.

IX. VERTEX RECONSTRUCTION

The vertex positions of signal-side decays of $B^0 \to K_S^0 \eta_{3\pi}\gamma$ and $B^0 \to K_S^0 \eta_{2\gamma}\gamma$ is determined from the charged tracks. For $B^0 \to K_S^0 \eta_{3\pi}\gamma$ decays, we require at least one of the charged pions from $\eta_{3\pi}$ decays, which originate from the B decay position, to have at least one (two) hit in the SVD $r - \phi$ (z) layers. To improve the B-vertex resolution, we use an additional constraint from the transverse-plane beam profile at the IP ($\sigma_x^{\text{beam}} \sim 100 \ \mu$m, $\sigma_y^{\text{beam}} \sim 5 \ \mu$m) smeared with the finite flight length of the B^0 meson in the $x - y$ plane. The estimated uncertainty of the reconstructed vertex position in the z direction (σ_z^{rec}) determined with single (two) charged track is required to be less than $500 \ \mu$m ($200 \ \mu$m) to ensure enough quality for time dependent analysis. For $B^0 \to K_S^0 \eta_{2\gamma}\gamma$ decays, the K_S^0 trajectory, reconstructed from its pion daughters, is used to determine the vertex position with the aforementioned constraint on the smeared beam profile; this strategy is adopted since the decay vertex of the long-lived K_S^0 is displaced from the B decay vertex. To have good resolution of the K_S^0 trajectory, both pions daughters must satisfy SVD-hit requirements of at least one (two) hit in the $r - \phi$ (z) layers for SVD1, and at least two hits in both $r - \phi$ and z layers for SVD2. We apply a selection on the σ_z^{rec} to be less than $500 \ \mu$m. The vertex position of B_{tag} is determined from well-reconstructed charged particles in the ROE [71]. The $|\Delta t|$ is restricted to be less than 70 ps for further analysis.

X. EVENT MODEL

We determine $\mathcal{S}$ and $\mathcal{A}$ by performing an unbinned maximum-likelihood fit to the observed Δt distribution in the signal region. The probability density function (PDF) expected for the signal distribution, $\mathcal{P}_{\text{sig}}(\Delta t, q, w_l, \Delta w_l; \mathcal{S}, \mathcal{A})$, is given by Eq. (2), modified to incorporate the effect of

incorrect flavor assignment. Two of the parameters in the PDF expression, τ_{B^0} and Δm_d, are fixed to their world average [72]. The distribution is convolved with the proper-time resolution function, $R_{\text{sig}}(\Delta t)$, which is a function of the event-by-event Δt uncertainties. The resolution function $R_{\text{sig}}(\Delta t)$ incorporates the detector resolution, contamination of nonprimary tracks in the vertex reconstruction of B_{tag}, and the kinematic energy generated by the $\Upsilon(4S)$ decay. As in Ref. [73], universal R_{sig} parameters are used for the vertex reconstruction for $\eta_{3\pi}$ and the long-lived K_S^0. A detailed description can be found in Ref. [74]. The PDF for $B\bar{B}$ background events ($\mathcal{P}_{B\bar{B}}$) is modeled in the same way as for signal, but with different lifetime and *CP* violation parameters while using the same resolution function ($R_{B\bar{B}} = R_{\text{sig}}$). The effective lifetime of the $B\bar{B}$ background is obtained from a fit to the MC sample for each η decay mode. The PDF for $q\bar{q}$ background events, $\mathcal{P}_{q\bar{q}}$, is modeled as the sum of exponential and prompt components, and is convolved with a double Gaussian representing the resolution function $R_{q\bar{q}}$. All parameters in $\mathcal{P}_{q\bar{q}}$ and $R_{q\bar{q}}$ are determined by a fit to the Δt distribution of a background-enhanced sample in the ΔE–M_{bc} sideband.

For each event i, the following likelihood function is calculated:

$$
\begin{aligned}
P_i = (1 - f_{\text{ol}}) \int & [f_{\text{sig}} \mathcal{P}_{\text{sig}}(\Delta t') R_{\text{sig}}(\Delta t_i - \Delta t') \\
& + f_{B\bar{B}} \mathcal{P}_{B\bar{B}}(\Delta t') R_{B\bar{B}}(\Delta t_i - \Delta t') \\
& + (1 - f_{\text{sig}} - f_{B\bar{B}}) \mathcal{P}_{q\bar{q}}(\Delta t') R_{q\bar{q}}(\Delta t_i - \Delta t')] d\Delta t' \\
& + f_{\text{ol}} \mathcal{P}_{\text{ol}}(\Delta t_i), \quad (4)
\end{aligned}
$$

where $\mathcal{P}_{\text{ol}}$ is a broad Gaussian function that represents an outlier component with a small fraction f_{ol} [74]. The signal and background probabilities, f_{sig} and $f_{B\bar{B}}$, are calculated on an event-by-event basis from the function obtained by the same ΔE–M_{bc}–$\mathcal{O}'_{\text{NB}}$ fit used to extract the signal yield, and are then multiplied by a factor that depends on the flavor tagging r-bin. The r distributions of the signal and the $q\bar{q}$ background are estimated by repeating the ΔE–M_{bc}–$\mathcal{O}'_{\text{NB}}$ fit procedure for each r interval with the three background shape parameters fixed to the full-range result. The $B\bar{B}$ background distribution is estimated from MC samples and found to be small.

XI. RESULTS

The only free parameters in the final fit are $\mathcal{S}$ and $\mathcal{A}$, which are determined by maximizing the likelihood function $L = \Pi_i P_i(\Delta t_i; \mathcal{S}, \mathcal{A})$, where the product is over all events. We obtain

$$\mathcal{S} = -1.32 \quad \text{and} \quad \mathcal{A} = -0.48$$

and find that the central values are outside of the physical boundary defined by $\mathcal{S}^2 + \mathcal{A}^2 = 1$. We extract the
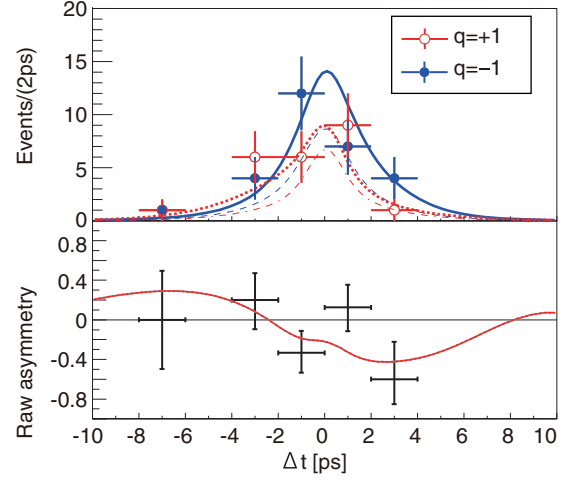

FIG. 4. Δt distribution (top) and raw asymmetry (bottom) for events in the $0.5 < r \le 1.0$ region. (Top) The filled blue dots show the distribution of $\bar{B}^0$ tagged events and the open red dots show the distribution for B^0 tagged events. The solid blue and dotted red curves show the total PDF for $\bar{B}^0$ and B^0 tagged events, respectively. The dashed blue and dot-dashed red curves represent the background PDF for $\bar{B}^0$ and B^0 tagged events, respectively. (Bottom) The solid red curve shows the result of the extended unbinned maximum-likelihood fit.

statistical uncertainties from the root-mean-square of the *CP* violation parameter distributions obtained using an ensemble test with input values of $(\mathcal{S}_{\text{true}}, \mathcal{A}_{\text{true}}) = (-0.94, -0.34)$, which is the closest point on the physical boundary to the fit result [75], as $\delta\mathcal{S} = \pm 0.77$ and $\delta\mathcal{A} = \pm 0.41$ [76]. The correlation between $\mathcal{S}$ and $\mathcal{A}$ is found to be 0.15. We define the raw asymmetry in each Δt interval as $(N_{q=+1} - N_{q=-1})/(N_{q=+1} + N_{q=-1})$, where $N_{q=\pm 1}$ is the number of observed candidates with the given q. The Δt distributions and raw asymmetries for events in the signal-enhanced $0.5 < r \le 1.0$ region for $q = \pm 1$ are shown in Fig. 4.

XII. VALIDATIONS

Various cross-checks are performed to confirm the validity of our procedure. The *CP* asymmetry fit to MC signal samples shows good linearity. Dedicated lifetime fits to $B^+ \to K^+ \eta \gamma$ samples yield 2.0 ± 0.3 ps and 2.3 ± 0.4 ps for $\eta_{2\gamma}$ and $\eta_{3\pi}$, respectively. A lifetime fit to $B^0 \to J/\psi K_S^0$ using only K_S^0 to determine the signal vertex results in 1.528 ± 0.027 ps. A *CP* asymmetry fit to the $B^+ \to K^+ \eta \gamma$ control samples yields $(\mathcal{S}, \mathcal{A}) = (0.01 \pm 0.35, 0.06 \pm 0.29)$ and $(0.2 \pm 0.6, 0.2 \pm 0.4)$ for $\eta_{2\gamma}$ and $\eta_{3\pi}$, respectively. Lastly, a *CP* asymmetry fit to $B^0 \to J/\psi K_S^0$ only using K_S^0 to determine the signal vertex position yields $(\mathcal{S}, \mathcal{A}) = (0.73 \pm 0.05, 0.00 \pm 0.03)$. These results are consistent with either their world-average or expected values [58].

TABLE I.   Systematic uncertainties of $\mathcal{S}$ and $\mathcal{A}$.

Source	$\mathcal{S}$	$\mathcal{A}$
Resolution parameters	± 0.257	± 0.049
Vertex reconstruction	± 0.232	± 0.022
Background Δt PDF	± 0.051	± 0.006
Flavor tagging	± 0.015	± 0.019
Physics parameters	± 0.004	± 0.002
PDF for 3D fit	± 0.096	± 0.024
CP violation in background	± 0.024	± 0.022
Possible fit bias	± 0.016	± 0.015
Tag-side interference	± 0.006	± 0.010
Total	± 0.364	± 0.068

XIII. SYSTEMATIC UNCERTAINTIES

We calculate systematic uncertainties in the following categories by fitting the data with each fixed parameter being varied by its uncertainty: values of physics parameters such as Δm_d and τ_{B^0}, effective lifetime and CP asymmetry of the $B\bar{B}$ background, imperfect knowledge of the $q\bar{q}$ background Δt PDF, the flavor-tagging determination, the signal and background fractions, and the resolution functions. A possible bias in the fit is checked by performing a large number of pseudo-experiments. The fit result is consistent with the input value within the statistical uncertainty. We quote this uncertainty as the possible fit bias. The uncertainty due to the vertex reconstruction is estimated by changing the requirements on the track quality. For the effect of SVD misalignment, we use the value from the latest $\sin 2\phi_1$ measurement at Belle [77], which is estimated from MC samples by artificially displacing the SVD sensors in a random manner. Effects of tag-side interference [78] are estimated with a control sample of $B \to D^* \ell \nu$ events. A detailed description of the evaluation of the systematic uncertainties is found in Ref. [79]. The dominant systematic contributions for $\mathcal{S}$ arise
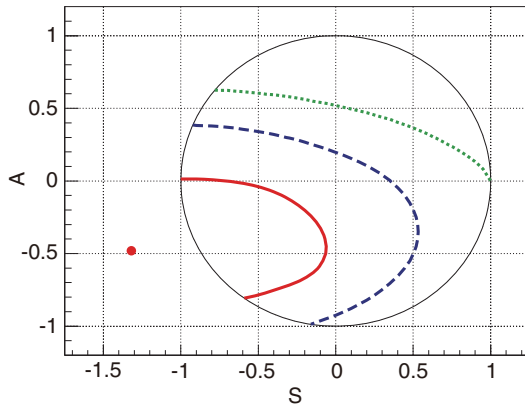

FIG. 5.   The solid red, dashed blue and dotted green curves show the 1σ, 2σ and 3σ confidence contours, respectively. The red dot shows the fit result. The physical boundary $\mathcal{S}^2 + \mathcal{A}^2 = 1$ is drawn with a thin solid black curve. Our result is consistent with a null asymmetry within 2σ.

from the uncertainties in the resolution function and vertex reconstruction. The systematic uncertainty in $\mathcal{A}$ is dominated by the resolution function. These contributions are added in quadrature and summarized in Table I.

XIV. CONFIDENCE LEVEL CONTOURS

Figure 5 shows confidence intervals calculated using the Feldman-Cousins frequentist approach [80], incorporating a smearing by additional Gaussian functions to represent the systematic uncertainties discussed above. Our result is less than 2σ away from zero, and is consistent with the *BABAR* result [44] as well as the SM predictions [48–53] with the assumption that time-dependent CP asymmetries in $B^0 \to K^{*0}\gamma$ and $B^0 \to K_S^0 \eta \gamma$ are the same.

XV. CONCLUSION

In summary, we have measured CP violation parameters in $B^0 \to K_S^0 \eta \gamma$ decays using a data sample of $772 \times 10^6 B\bar{B}$ pairs. The obtained parameters,

$$\mathcal{S} = -1.32 \pm 0.77(\text{stat}) \pm 0.36(\text{syst}),$$
$$\mathcal{A} = -0.48 \pm 0.41(\text{stat}) \pm 0.07(\text{syst}),$$

are consistent with the null-asymmetry hypothesis within 2σ as well as with SM predictions [48–53]. Our measurement is dominated by statistical uncertainty. Therefore, with much higher statistics and also higher acceptance and reconstruction efficiencies, the forthcoming Belle II experiment should significantly improve upon the precision of this measurement.

[1] S. Chen *et al.* (CLEO Collaboration), Phys. Rev. Lett. **87,** 251807 (2001).

[2] B. Aubert *et al.* (*BABAR* Collaboration), Phys. Rev. D **77,** 051103 (2008).

[3] J. P. Lees *et al.* (*BABAR* Collaboration), Phys. Rev. Lett. **109,** 191801 (2012).

[4] J. P. Lees *et al.* (*BABAR* Collaboration), Phys. Rev. D **86,** 052012 (2012).

[5] A. Limosani *et al.* (Belle Collaboration), Phys. Rev. Lett. **103,** 241801 (2009).

[6] T. Saito *et al.* (Belle Collaboration), Phys. Rev. D **91,** 052004 (2015).

[7] T. Becher and M. Neubert, Phys. Rev. Lett. **98,** 022003 (2007).

[8] M. Misiak *et al.*, Phys. Rev. Lett. **114,** 221801 (2015).

[9] See, for example, U. Haisch and A. Weiler, Phys. Rev. D **76,** 034014 (2007); A. Freitas and U. Haisch, Phys. Rev. D **77,** 093008 (2008); M. Blanke, A. J. Buras, K. Gemmler, and T. Heidsieck, J. High Energy Phys. 03 (2012) 024; K. Ishiwata, N. Nagata, and N. Yokozaki, Phys. Lett. B **710,** 145 (2012); W. Altmannshofer, M. Carena, N. R. Shah, and F. Yu, J. High Energy Phys. 01 (2013) 160; M. Misiak and M. Steinhauser, Eur. Phys. J. C **77,** 201 (2017).

[10] P. Ramond, Phys. Rev. D **3,** 2415 (1971).

[11] Y. A. Golfand and E. P. Likhtman, Pis'ma Zh. Eksp. Teor. Fiz. **13,** 452 (1971) [JETP Lett. **13,** 323 (1971)].

[12] A. Neveu and J. H. Schwarz, Nucl. Phys. **B31,** 86 (1971).

[13] J. L. Gervais and B. Sakita, Nucl. Phys. **B34,** 632 (1971).

[14] D. V. Volkov and V. P. Akulov, Phys. Lett. **46B,** 109 (1973).

[15] J. Wess and B. Zumino, Nucl. Phys. **B70,** 39 (1974); Phys. Lett. **49B,** 52 (1974).

[16] R. N. Mohapatra and J. C. Pati, Phys. Rev. D **11,** 566 (1975); G. Senjanovic and R. N. Mohapatra, Phys. Rev. D **12,** 1502 (1975).

[17] L. Randall and R. Sundrum, Phys. Rev. Lett. **83,** 3370 (1999).

[18] W. D. Goldberger and M. B. Wise, Phys. Rev. D **60,** 107505 (1999); Phys. Rev. Lett. **83,** 4922 (1999).

[19] H. Davoudiasl, J. L. Hewett, and T. G. Rizzo, Phys. Lett. B **473,** 43 (2000).

[20] A. Pomarol, Phys. Lett. B **486,** 153 (2000).

[21] S. Chang, J. Hisano, H. Nakano, N. Okada, and M. Yamaguchi, Phys. Rev. D **62,** 084025 (2000).

[22] T. Gherghetta and A. Pomarol, Nucl. Phys. **B586,** 141 (2000).

[23] K. Fujikawa and A. Yamada, Phys. Rev. D **49,** 5890 (1994).

[24] P. L. Cho and M. Misiak, Phys. Rev. D **49,** 5894 (1994).

[25] K. S. Babu, K. Fujikawa, and A. Yamada, Phys. Lett. B **333,** 196 (1994).

[26] L. L. Everett, G. L. Kane, S. Rigolin, L. T. Wang, and T. T. Wang, J. High Energy Phys. 01 (2002) 022.

[27] K. Agashe, G. Perez, and A. Soni, Phys. Rev. Lett. **93,** 201804 (2004).

[28] D. Atwood, M. Gronau, and A. Soni, Phys. Rev. Lett. **79,** 185 (1997).

[29] D. Atwood, T. Gershon, M. Hazumi, and A. Soni, Phys. Rev. D **71,** 076003 (2005).

[30] N. Cabibbo, Phys. Rev. Lett. **10,** 531 (1963).

[31] M. Kobayashi and T. Maskawa, Prog. Theor. Phys. **49,** 652 (1973).

[32] C. K. Chua, X. G. He, and W. S. Hou, Phys. Rev. D **60,** 014003 (1999).

[33] E. J. Chun, K. Hwang, and J. S. Lee, Phys. Rev. D **62,** 076006 (2000).

[34] C. K. Chua, W. S. Hou, and M. Nagashima, Phys. Rev. Lett. **92,** 201803 (2004).

[35] T. Goto, Y. Okada, T. Shindou, and M. Tanaka, Phys. Rev. D **77,** 095010 (2008).

[36] P. Ko, J. h. Park, and M. Yamaguchi, J. High Energy Phys. 11 (2008) 051.

[37] M. Blanke, B. Shakya, P. Tanedo, and Y. Tsai, J. High Energy Phys. 08 (2012) 038.

[38] Y. Shimizu, M. Tanimoto, and K. Yamamoto, Phys. Rev. D **87**, 056004 (2013).

[39] E. Kou, C. D. Lü, and F. S. Yu, J. High Energy Phys. 12 (2013) 102.

[40] N. Haba, H. Ishida, T. Nakaya, Y. Shimizu, and R. Takahashi, J. High Energy Phys. 03 (2015) 160.

[41] R. Malm, M. Neubert, and C. Schmell, J. High Energy Phys. 04 (2016) 042.

[42] Y. Ushiroda *et al.* (Belle Collaboration), Phys. Rev. D **74**, 111104 (2006).

[43] B. Aubert *et al.* (*BABAR* Collaboration), Phys. Rev. D **78**, 071102 (2008).

[44] B. Aubert *et al.* (*BABAR* Collaboration), Phys. Rev. D **79**, 011102 (2009).

[45] J. Li *et al.* (Belle Collaboration), Phys. Rev. Lett. **101**, 251601 (2008).

[46] P. del Amo Sanchez *et al.* (*BABAR* Collaboration), Phys. Rev. D **93**, 052013 (2016).

[47] H. Sahoo *et al.* (Belle Collaboration), Phys. Rev. D **84**, 071101 (2011).

[48] B. Grinstein, Y. Grossman, Z. Ligeti, and D. Pirjol, Phys. Rev. D **71**, 011504 (2005).

[49] B. Grinstein and D. Pirjol, Phys. Rev. D **73**, 014013 (2006).

[50] M. Matsumori and A. I. Sanda, Phys. Rev. D **73**, 114022 (2006).

[51] P. Ball and R. Zwicky, Phys. Lett. B **642**, 478 (2006).

[52] P. Ball, G. W. Jones, and R. Zwicky, Phys. Rev. D **75**, 054004 (2007).

[53] S. Jäger and J. Martin Camalich, Phys. Rev. D **93**, 014028 (2016).

[54] A. Abashian *et al.* (Belle Collaboration), Nucl. Instrum. Methods Phys. Res., Sect. A **479**, 117 (2002); also see detector section in J. Brodzicka *et al.*, Prog. Theor. Exp. Phys. **2012**, 04D001 (2012).

[55] S. Kurokawa and E. Kikutani, Nucl. Instrum. Methods Phys. Res., Sect. A **499**, 1 (2003), and other papers included in this volume; T. Abe *et al.*, Prog. Theor. Exp. Phys. (**2013**) 03A001 and references therein.

[56] Z. Natkaniec *et al.* (Belle SVD2 Group), Nucl. Instrum. Methods Phys. Res., Sect. A **560**, 1 (2006).

[57] P. Koppenburg *et al.* (Belle Collaboration), Phys. Rev. Lett. **93**, 061803 (2004).

[58] C. Patrignani *et al.* (Particle Data Group), Chin. Phys. C **40**, 100001 (2016) and (2017) update.

[59] NeuroBayes software package based on Bayesian statistics, in M. Feindt and U. Kerzel, Nucl. Instrum. Methods Phys. Res., Sect. A **559**, 190 (2006).

[60] H. Nakano, Ph.D Thesis, Tohoku University, 2014, Chap. 4, unpublished, https://tohoku.repo.nii.ac.jp/?action=pages_view_main&active_action=repository_view_main_item_detail&item_id=70563&item_no=1&page_id=33&block_id=38.

[61] The Fox-Wolfram moments were introduced, in G. C. Fox and S. Wolfram, Phys. Rev. Lett. **41**, 1581 (1978).

[62] S. H. Lee *et al.* (Belle Collaboration), Phys. Rev. Lett. **91**, 261801 (2003).

[63] J. D. Bjorken and S. J. Brodsky, Phys. Rev. D **1**, 1416 (1970).

[64] R. Brun *et al.*, GEANT, CERN Report No. DD/EE/84-1, 1984.

[65] Throughout this paper, the inclusion of the charge conjugate mode decay is implied unless otherwise stated.

[66] Recently, first evidence for isospin violation was reported in a decay mediated by the $b \to s\gamma$ process, $B \to K^*\gamma$ [67]. This result is consistent with the SM prediction of small isospin breaking.

[67] T. Horiguchi *et al.* (Belle Collaboration), Phys. Rev. Lett. **119**, 191802 (2017).

[68] R. Aaij *et al.* (LHCb Collaboration), Phys. Rev. Lett. **113**, 162001 (2014).

[69] H. Albrecht *et al.* (ARGUS Collaboration), Phys. Lett. B **241**, 278 (1990).

[70] H. Kakuno *et al.*, Nucl. Instrum. Methods Phys. Res., Sect. A **533**, 516 (2004).

[71] K. F. Chen *et al.* (Belle Collaboration), Phys. Rev. D **72**, 012004 (2005).

[72] J. Beringer *et al.* (Particle Data Group), Phys. Rev. D **86**, 010001 (2012).

[73] K. Sumisawa *et al.* (Belle Collaboration), Phys. Rev. Lett. **95**, 061801 (2005).

[74] H. Tajima *et al.*, Nucl. Instrum. Methods Phys. Res., Sect. A **533**, 370 (2004).

[75] K. Abe *et al.* (Belle Collaboration), Phys. Rev. D **68**, 012001 (2003).

[76] We repeated the ensemble test with the input values of $(\mathcal{S}_{\text{true}}, \mathcal{A}_{\text{true}}) = (0.00, 0.00)$. The sensitivities are $(\delta\mathcal{S}, \delta\mathcal{A}) = (\pm 0.59, \pm 0.34)$ which are smaller than the uncertainties quoted in the text.

[77] I. Adachi *et al.* (Belle Collaboration), Phys. Rev. Lett. **108**, 171802 (2012).

[78] O. Long, M. Baak, R. N. Cahn, and D. P. Kirkby, Phys. Rev. D **68**, 034010 (2003).

[79] L. Šantelj *et al.* (Belle Collaboration), J. High Energy Phys. 10 (2014) 165.

[80] G. J. Feldman and R. D. Cousins, Phys. Rev. D **57**, 3873 (1998).